Quarterly Report: 3rd Quarter (April 1 2016 – June 30 2016)

1	**Deviations from plan**
	None to report for this quarter
2	**Progress made since last reporting**
	This is the third quarterly report for this project. The progress made during this time are listed below. The team is progressing as per schedule on all of the tasks. Details are provided below. Work towards several deliverables are ongoing. None of the tasks are delayed at this point.
3	**Published deliverables and achieved milestones**
	PCM selection (both microencapsulated and liquid) has been completed, as is the characterization of thermophysical properties of the PCMs and their dispersion in cement pastes. The quantification of PCM incorporation in porous hosts also has been completed
4	**Any problems that occurred and solutions found**
	No problems have occurred in the first quarter of this project.
5	**Financial Progress**
	The partner universities and organizations have been provided the respective share of the pre-financing amount, and the coordinator is monitoring the progress carefully. The project manager for ECLIPS, Lisa Schulze at Arizona State University is overseeing the financial progress and other aspects between all partners.

The following activities have been carried out in Quarter 3 of the project. They are detailed below, based on the work packages that they belong to. The work performed in this quarter is a continuation from the previous quarter.

WP1: Selection, characterization and optimization of PCMs and delivery strategies:

a) Encapsulating PCMs in silica capsules:

The goal of this WP is to obtain microencapsulated PCMs in silica capsules. In the previous report we described the PCMs chosen based on the applications sought for in the project to be encapsulated. For the lower range we suggested a PEG compound, PEG 400 MM, which has a melting point at around 4ºC and a heat of fusion (ΔH_f) of 49 J/g. Since then we have found another candidate, a paraffin base compound, tetradecane, which has a higher heat of fusion and might be more interesting to encapsulate. Figure 1 shows the differential scanning calorimetry (DSC) spectrum of tetradecane.

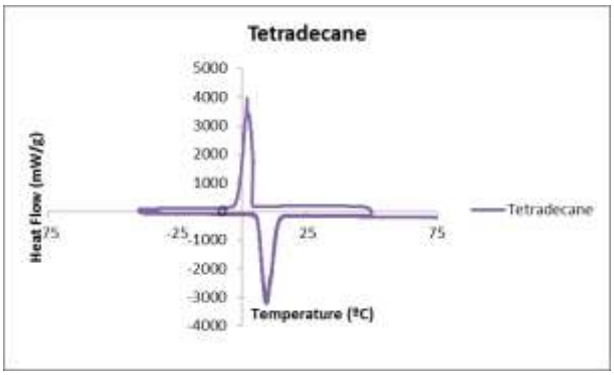

Figure 1: DSC scan of tetradecane. The endothermic part of the spectrum gives the melting temperature obtained (T=9.33ºC) and the heat of fusion (ΔH_f=183.3 J/g).

Encapsulation of heptadecane (Tm=22ºC): In the previous report we described the reactions carried out to encapsulate the compound heptadecane. A sol-gel reaction was used where in a first step the hydrolysis of the alkoxysilane is carried out followed by an emulsion and condensation step. Following this synthetic path we were able to obtain silica capsules that contain heptadecane. However, some of the capsules appeared to be broken and the shells showed certain porosity. We are working to improve the encapsulation and for that we are studying the addition of different surfactants as well as other synthetic routes (with other alkoxysilanes and condensation agents instead of HCl and NH_4OH). In Table 1 some of the experiments done following different synthetic routes are shown.

Table1. Different synthetic routes carried out for the improvement of the heptadecane encapsulation

Ref	Starting material (alkoxysilane)	PCM	Hydrolysis/condensation agent	Surfactant	Comments	Article
Rxn type 1	Tetraethoxysilane (TEOS)	heptadecane	HCl 37% (conc.)	DTMAB	amorphous material, small (<1μm) spherical particles, difficult to filter/isolate	J. of Microencapsulation 2006, 23(1), 3-14
Rxn type 2	TEOS	heptadecane	acetic acid	polyvinyl alcohol, Span 80, Tween 80	amorphous material obtained	Chem. Lett. 2007, 36(4), 494
Rxn type 3	methyltrimethoxysilane (MTMS); 3-aminopropyltriethoxysilane	heptadecane	3-aminopropyltriethxysilane	–	small (<1μm) spherical particles were obtained, difficult to isolate	Chem. Lett. 2006, 35(6), 622
Rxn type 4	TEOS	heptadecane	3-aminopropyltriethxysilane	–	small (<1μm) spherical particles were obtained difficult to isolate	Chem. Lett. 2006, 35(6), 622
Rxn type 5	MTMS, 3-aminopropyltriethoxysilane	heptadecane	3-aminopropyltriethxysilane	Span 80, Tween 80	small (<1μm) spherical particles were obtained difficult to isolate	Chem. Lett. 2006, 35(6), 622
Rxn type 6	TEOS	heptadecane	HCl 2M	Span 80, Tween 80	amorphous material and most of the PCM is not encapsulated	Colloids and Surfaces A: Physicochemical and Engineering Aspects 2011, 389, 104-117

In some of these experiments amorphous material was formed and in almost all cases the separation of the solid from the reaction dispersion was difficult. In several of the reactions very small, lower than 1 μm, spherical particles were obtained. For example, the size of the spherical particles are around 500 nm as it can be seen in the scanning electron microscopy images shown in Figure 2. It is not very clear from these images whether these particles are hollow and if they contain the heptadecane inside, but when the product is characterized by FTIR, absorption bands due to the PCM can be seen as well as due to the silica of the shells which indicate that there is some organic material in the product. However, for the application intended, larger particle diameter is more suited since bigger microcapsules can contain a larger amount of phase change material and so they could show a bigger effect once they are introduced in the cement-based matrix. Taking this into account we are still going to keep investigating other synthetic avenues to try to improve the encapsulation of heptadecane.

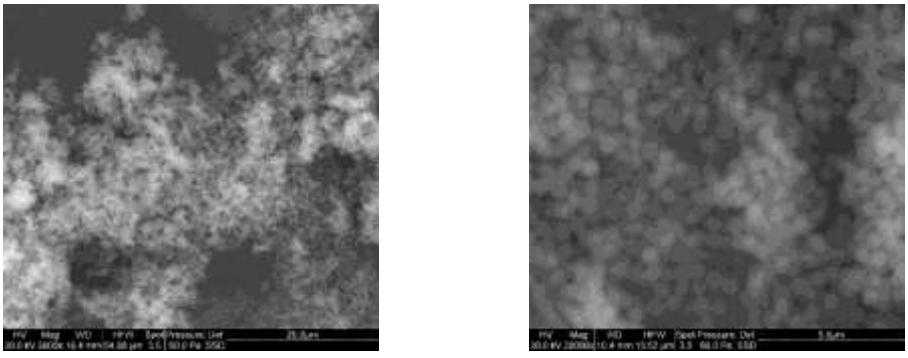

Figure 2: Scanning electron microscopy images of the nanometric spherical particles.

Encapsulation of Paraffin wax (Tm=53-57ºC): In this period we have also started analyzing the encapsulation of the paraffin wax (purchased from Sigma-Aldrich, characteristics: C_nH_{2n+2}, n=24-26, Tm=53-57ºC and ΔH_f= 250 J/g according to literature). For the encapsulation of the paraffin wax we have started with the sol-gel reaction. In this case however, the paraffin is solid at room temperature and so we have increased the emulsion temperature (the second part of the reaction) between 60-70ºC to melt the paraffin and this way to be able to form the emulsion process and encapsulate it in the silica shell. Reactions were carried out at different temperatures (e.g., 60ºC, 65ºC and 70ºC). In Figure 3, scanning electron microscopy images of the material obtained are shown. Some of the particles are broken and it can be seen that another material is flowing out from the capsule. This suggests that the paraffin wax has been successfully encapsulated. However, when X-ray dispersive analysis (EDAX) is used to do the elemental analysis we can see that some of the areas contain more silicon than other areas and in the low silicon content zone the carbon signal is more intense. This seems to indicate that there is some paraffin outside the capsules which needs to be removed.

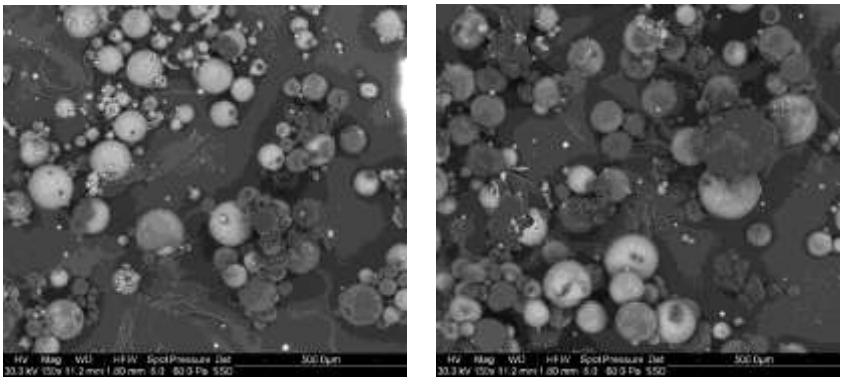

Figure 3: Scanning electron images of the product obtained in the encapsulation of paraffin wax. Different diameter size particles can be seen, some as large as 250 µm.

b) Impregnating porous hosts with PCMs:

Four different lightweight aggregates (LWAs) as explained in the previous report were used to impregnate them with a PCM having a phase change temperature of 24°C. The PCMs were impregnated into the LWAs at ambient temperature and pressure. Vacuum saturation was not adopted to ensure that the process is practically feasible. The PCM impregnation capacity of the LWAs depends on the pore structure features of the LWAs. Figure 4(a) shows the pore volume intruded by mercury for all the aggregates. However the available pore volume and absorption are not the same, because of unconnected pores in the aggregates. This necessitated separate determinations of the PCM absorption capacity. Figure 4(b) shows the endothermic heat flow peak for the four different LWAs impregnated with PCM (up to their absorption capacity), after 72 hours of absorption. The endothermic peak represents the heat being absorbed by the PCM (latent energy storage), as a result of phase transition. The onset temperature (T_{onset}) corresponding to melting is 17.3 $\pm$ 0.2°C and the completion temperature ($T_{completion}$) is 27.5 $\pm$ 0.2°C. The melting point or endothermic peak occurs at 24°C for all the LWA-PCM combinations, i.e., at the intrinsic PCM phase change temperature. The difference in heat flow curves between different LWA-PCM combinations is a result of the differences in the PCM absorption capacity of the LWA. The mortar samples were proportioned for a constant paste volume of 50%. The LWA mortars contained 50% LWA by volume. For the LWA mortars, 5% PCM by overall volume of the mortar was incorporated by adjusting the amount of LWA impregnated by the PCM. This is illustrated in Figure 4(c) using the case of perlite aggregates as an example.

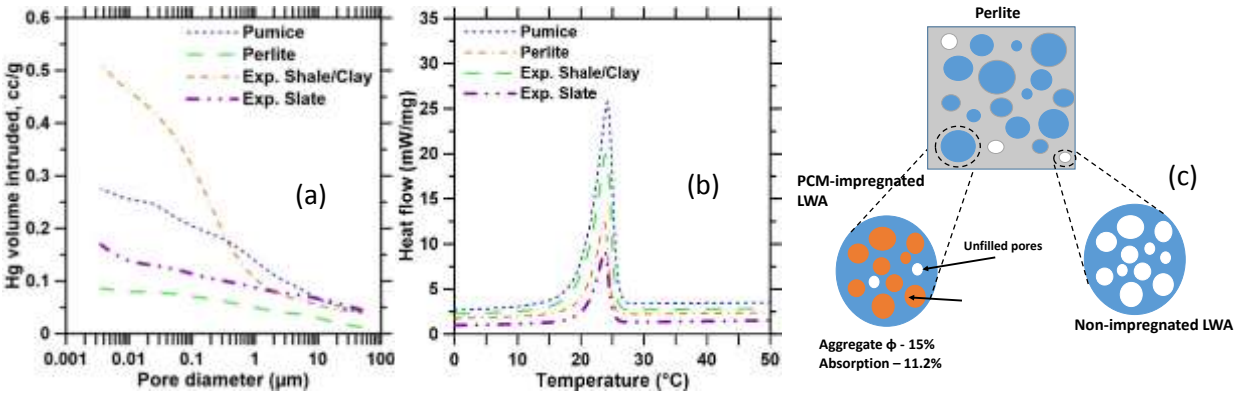

Figure 4: (a) Pore volume intruded for the different LWAs, (b) DSC scans of the different LWAs impregnated with PCMs, and (c) illustration of the mixture design method to contain 5% of PCM by volume of the mortar

The thermal conductivity of all the mortars evaluated here are shown in Figure 5. PCM impregnated LWA mortars generally show thermal conductivities that are about 10%-to-20% lower than the regular LWA (water-saturated) mortars, at a total PCM content of 5% by volume in the mortars. This reduction in thermal conductivity can be attributed to the lower thermal conductivity of the PCM (0.15 W/m-K) as compared to that of water (0.6 W/m-K). In addition, the absorption capacity of the LWA also influences the thermal conductivity since the pores that are not accessible to water and/or PCM are filled with air that has a much lower thermal conductivity than any of the other constituents.

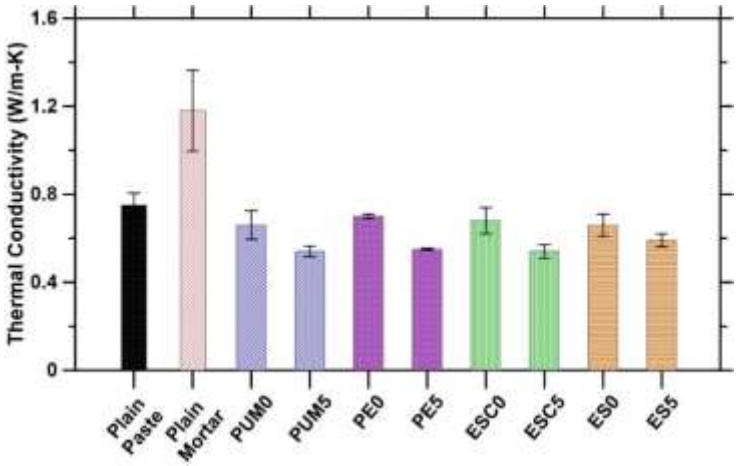

Figure 5: Thermal conductivity determined after 28 days of hydration for the paste and mortars. The first data is for OPC paste, and the rest are for mortars where the paste volume fraction is 0.50.

WP2 and WP3: PCM-cement composites: Microstructural and thermomechanical properties, and PCM-Concrete Mixture Design

In the 3rd quarter, work has been performed on studying the influence of PCM microcapsule addition on (micro)mechanical properties of cement based materials. First part included investigating the influence of temperature (i.e. below or above phase change temperature) on the properties of PCM microcapsules. For this purpose, nanoindentation technique was used. A flat tip with a diameter of 135 microns was used

(Figure 6). Microcapsules were sprinkled on top of a stage and individual microcapsules were identified and subjected to loading (Figure 7). From the force-displacement diagram, it was possible (although *not always*) to determine the maximum load that each capsule could sustain. This was repeated for room-temperature conditions (>25 degrees Celsius, above the phase change temperature), and for 15 degrees Celsius using a temperature stage (below the phase change temperature). A trend of higher strength of PCM microcapsules under lower temperatures was identified (Figure 8).

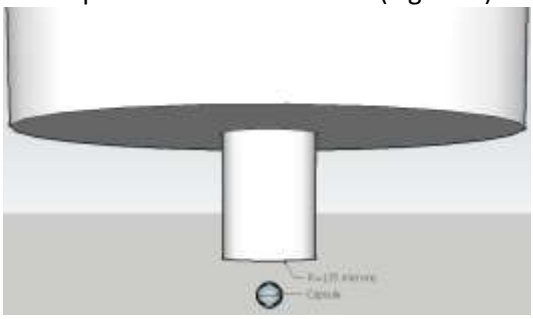

Figure 6: Nanoindentation setup used to measure the force-displacement relationship of PCM microcapsules

Figure 7: A single PCM microcapsule before (left) and after (right) the nanoindentation test

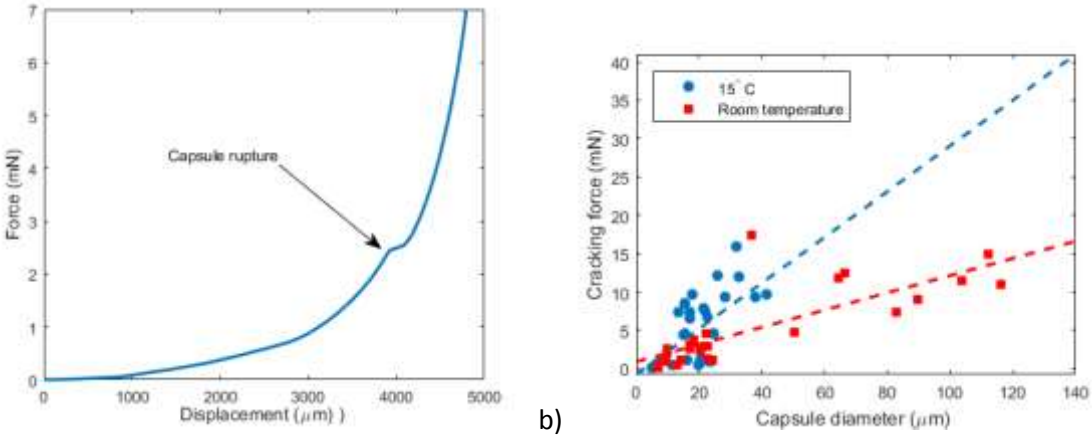

a) b)

Figure 8: a) Typical force-displacement diagram for a PCM microcapsule[1]; b) A relationship between capsule diameter and cracking force for two tested temperature regimes.

[1] Koopman, M., Gouadec, G., Carlisle, K., Chawla, K. K., & Gladysz, G. (2004). Compression testing of hollow microspheres (microballoons) to obtain mechanical properties. Scripta Materialia, 50(5), 593-596.

Following this experiment, it was decided to focus on the influence of PCM microcapsules on the micromechanical properties of PCM-cement composites. In particular, the focus is on the two opposing changes caused by the PCM microcapsule addition: (1) first, soft inclusions in the matrix will cause a decrease in strength/modulus (2) due to their small size, the microcapsules may act as nucleation sites for hydration thereby improving the (micro)mechanical properties.

First, micromechanical properties of cement pastes (w/c=0.45, CEM I 42.5 N, 0-30% PCM microcapsules per volume) were tested using nanoindentation technique (CSM method with a Berkovich tip). In Figure 9, a summary of test results for 3-day old pastes is given. Currently, more tests are ongoing for ages of 7 and 28 days to determine how the micromechanical properties develop in time depending on the PCM volume. In addition, porosity measurements and TGA will be performed and results evaluated to determine how the synergy of the two aforementioned processes affects the mechanical performance of the cement paste phase in concrete.

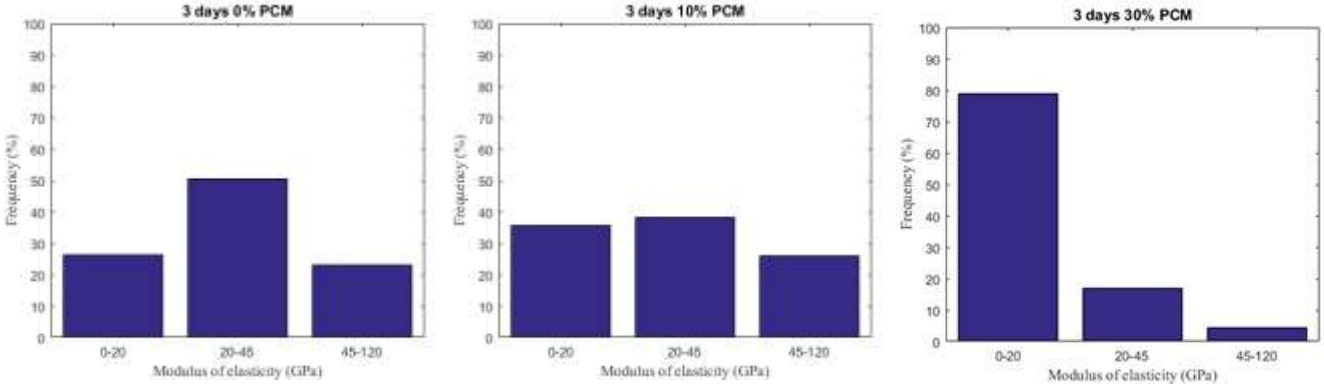

Figure 9: Nanoindentation results of 3-day old cement pastes

WP4: Numerical modeling of thermal evolution

Figure 10 shows a schematic of the one-dimensional heat transfer model used to estimate the transient temperature evolution along the thickness of the pavement. The model assumes a realistic pavement thickness of L = 25 cm. The upper surface of the pavement is exposed to the outdoor temperature and solar irradiation, and exchanges heat by radiation with the atmosphere. The composite pavement material has effective thermal properties k_{eff} and $(\rho c_p)_{eff}(T)$. The PCM, chosen here, has a melting temperature of 25°C. In the early-age, the pavement section experiences volumetric heat generation $\dot{q}(x,t)$ due to the exothermic hydration of cement. The time and temperature dependence of heat generation are quantified using equivalent age, based on our experimental data from isothermal calorimetry. Below the pavement section is a soil section with a constant ground temperature (T_g) at its bottom interface (L_s).

To study the effect of pouring time on early age heat generation, we consider two realistic concrete pouring times of 6 am and 6 pm. For the pouring time of 6 am, the transient temperature evolutions within pavement sections with (a) plain concrete, and (b) concrete containing 10% microencapsulated PCM by volume (ϕ_{c+s} = 0.1) are plotted in Figure 11. The temperatures represent: (i) the pavement surface (x = 0 m), (ii) half-depth (x = L/2), and (iii) the pavement-soil interface (x = L). The outdoor temperature and solar irradiation conditions correspond to a hot September day in Los Angeles, CA. From the figure, we observe a significant temperature rise in the half-depth and surface, and a large difference between the half-depth and soil interface temperatures. This is because the high outdoor temperature and solar irradiation at mid-day coincide with the bulk of heat generation due to hydration within the pavement.

The addition of PCM (Figure 11b) reduces the maximum temperature by ≈ 3°C. Note that the melting temperature of PCM used in this case is 25°C. As such, this temperature reduction is due to larger specific heat capacity and reduced thermal conductivity in the composite, rather than the latent heat storage. Thus, the choice of PCM with an appropriate melting temperature, depending on the ambient conditions, is an important criterion to achieve efficient temperature reduction.

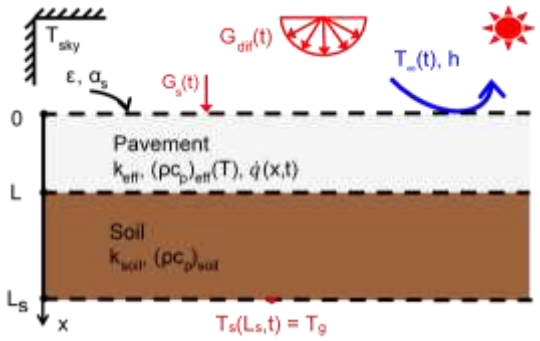

Figure 10: Schematic of the heat transfer model consisting of a pavement section of length L exposed to the ambient air and a soil section with a constant ground temperature at its bottom surface.

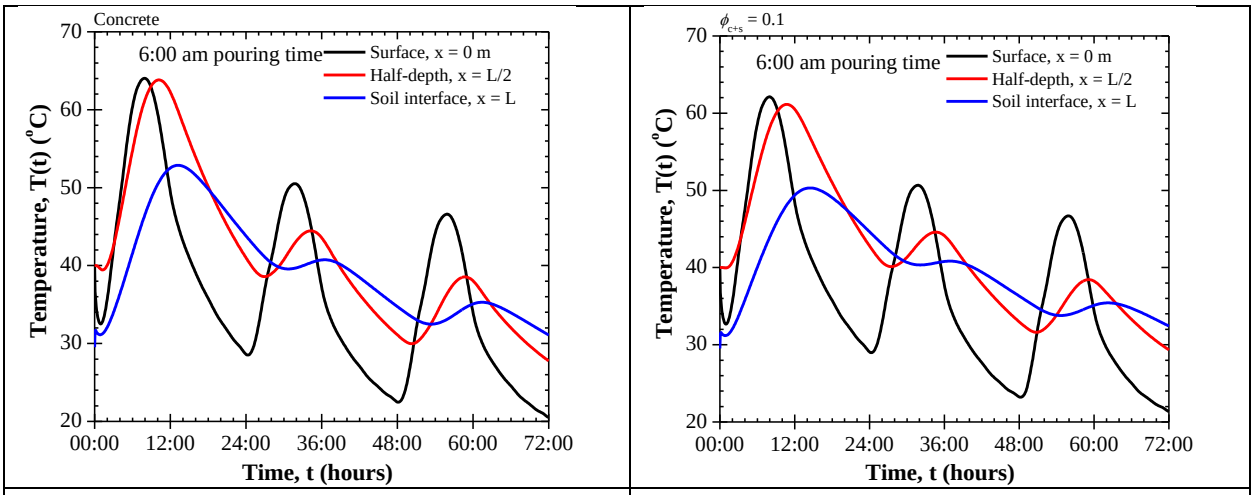

Figure 11: Transient temperature evolutions within pavement sections composed of (a) plain concrete, and (b) concrete containing PCM (ϕ_{c+s} = 0.1). The pavements were poured at 6:00 am and exposed to outdoor temperature and solar radiation corresponding to a hot September day in Los Angeles, CA.

Figure 12 shows temperature evolutions for a pouring time of 6:00 pm. In this case, the bulk of heat generation occurs before the high heat of the next day and thus, we observe two distinct maxima of the half-depth temperature within the first 24 hours of pouring. The maximum temperature developed in the pavement is significantly reduced compared to a pouring time of 6:00 am, reducing the potential risks of early-age cracking. However, PCMs are found to have little effects on reducing the thermal inertia in this case. These results indicate that the time of pouring concrete is a critical parameter to evaluate the potential benefits of PCM dosage in a pavement section.

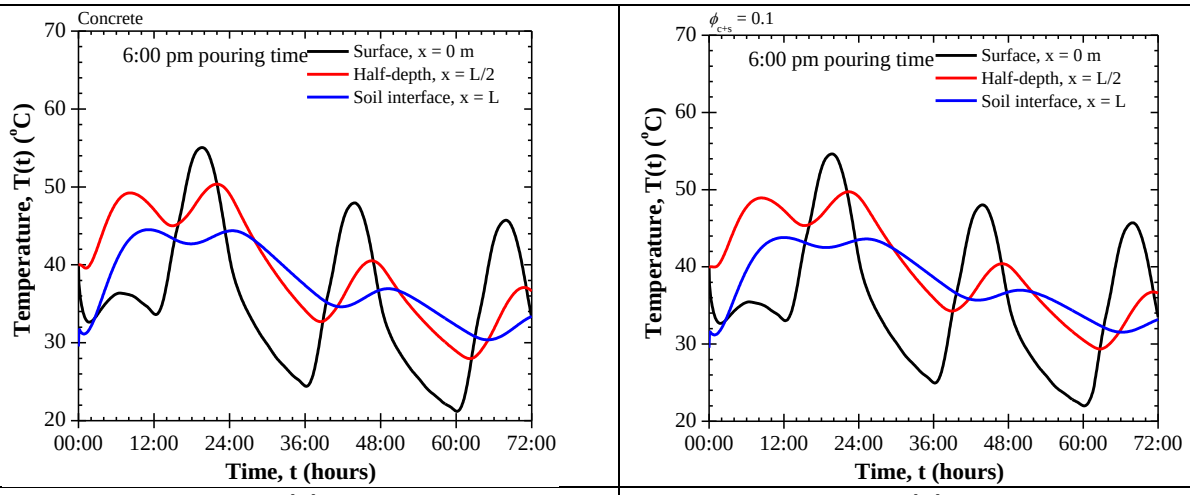

Figure 12: Transient temperature evolutions within pavement sections composed of **(a)** plain concrete, and **(b)** concrete containing PCM (ϕ_{c+s} = 0.1). Identical outdoor temperature and solar radiation conditions to Figure 2 were utilized, but pouring time was shifted to 6:00 pm.

Overall, through the heat transfer model we have identified two critical parameters which govern the efficiency of PCM in mitigating thermal cracking, other than the PCM dosage: 1) concrete pouring time, 2) melting temperature of PCM. In the future work, we will identify more rigorous performance metrics (e.g., maximum local temperature gradient) to quantify the effects of PCM as a function of (i) PCM dosage, (ii) PCM melting temperature, (iii) pouring time, and (iv) surface boundary conditions.

WP5: Cracking sensitivity and deformability response

In order to determine the temperature at which the PCM exhibit the phase change, PCM from the delivery in October 2015 (9914) and February 2016 (0037) were filled in a cylindrical container (Ø = 50 mm, height = 65 mm) equipped with thermo-elements and stored in a fridge at 10 °C. Afterwards, they were moved into an oven. The oven was started with the temperature set to 35 °C. The PCM start with the phase change at a temperature of approximately 17 °C, as indicated by the development of temperature in the containers with a decrease of the temperature gradient (Figure 13). The phase change seems to be completed at a temperature of 22-23 °C.

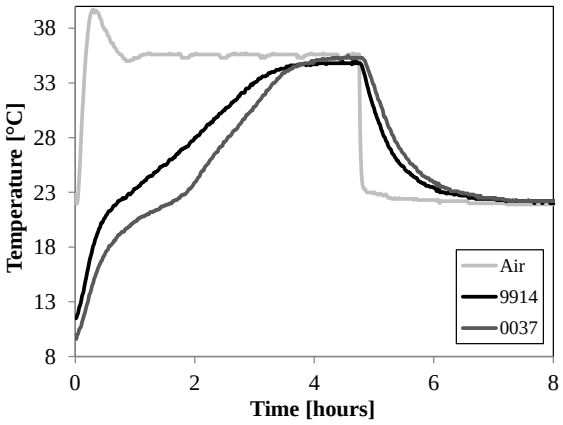

Figure 13: Temperature as a function of time of the air in the oven and the two PCM (9914 and 0037).

In the next step, the aim was to determine the mechanical properties of mortars containing PCM and to compare them to a reference mortar. Three mortar mixtures were produced: a reference mixture (M-Ref) and two mixtures containing PCM (Table 1). As aggregate alluvial sand and gravel was used. The cement was a CEM I 52.5 R. As superplastizicer Sika Viscocrete 20HE was used. In one mortar sand 0/1 mm was replaced by PCM in an amount corresponding to 20 volume-% of the cement volume (M-S20). In the other mortar cement was replace by the same volume (M-C20). Prisms (12 x 12 x 36 cm^3) were produced to determine the following mechanical properties:

From the data obtained so far, partial replacement of sand by PCM results in a decrease of compressive strength and E-modulus of concrete. The higher relative decrease of E-modulus compared to compressive strength might be beneficial for risk of cracking. Replacing cement with PCM results in a significant decrease of both compressive strength and E-modulus. While such a response is not noted for mortars, it is anticipated that the larger aggregates and their movements result in breakage of microcapsules, causing strength reduction. Efforts are underway to mitigate this problem.

WP8: Knowledge Management and Dissemination

- The first ECLIPS newsletter has been disseminated through the partners and several other networks
- A technote is being prepared
- Research publications are being prepared by partner institutions based on the respective work
- The ECLIPS website is being filled with content. (http://eclips.asu.edu)